Star Tracker-Based Acquisition, Tracking, and Pointing Technology for Deep-Space Optical Communications

S. Lee,[1] G. G. Ortiz,[1] and J. W. Alexander[2]

This article presents the concept and estimates of the pointing-knowledge accuracy of a star tracker-based acquisition, tracking, and pointing system. The major advantages of this technology are (1) no requirement for a costly ground-based laser beacon, (2) a large mission range beyond the solar system, and (3) a heritage of mature star tracker technology. The key concept is to combine high-accuracy star trackers and high-bandwidth inertial sensors to achieve high-accuracy and high-bandwidth pointing knowledge through the iterative averaging process. The pointing-knowledge bandwidth is divided into three areas (0–10 Hz, 10–50 Hz, and >50 Hz). Signal for each bandwidth are provided by star tracker gyros and angle sensors. Analysis shows that a pointing knowledge of 150 nanoradians (single axis, 1 sigma) can be achieved with an 8-cm-diameter telescope aperture. Additional expectations include 1/25 pixel accuracy per star, Space Infrared Telescope Facility (SIRTF)-class gyros (ARW = 0.0001 deg/root-hr), 5-Hz star trackers with an ∼5.0 degree field of view, a detector of 1000 by 1000 pixels, and stars of roughly 9 to 9.5 magnitudes. This 150-nanoradian pointing knowledge is well below the typical deep-space optical communications requirements of 200 to 300 nanoradians. Furthermore, the link availability can be maintained above 98 percent with a single star tracker.

I. Introduction

Optical communications is a technology that potentially can provide very high data rates from deep space. However, this requires pointing a communications laser to an Earth-based receiving station with sub-microradian accuracy. One major technology challenge is to achieve the pointing knowledge that is required to be much more accurate than the pointing accuracy. This must be accomplished over a wide bandwidth that can be used for the controller that compensates the external disturbances (e.g., spacecraft vibration) with a pointing servo control.

---

[1] Communications Architectures and Research Section.

[2] Inner Planet Flight Dynamics Section.

The research described in this publication was carried out by the Jet Propulsion Laboratory, California Institute of Technology, under a contract with the National Aeronautics and Space Administration.

In the existing schemes, a ground-based laser beacon has been used as the reference to estimate the pointing knowledge [1]. This is the only demonstrated acquisition, tracking, and pointing (ATP) technology for optical communications in space [2] and also the baseline for the future deep-space optical communications experiment, the Mars Laser Communications Demonstrator (MLCD), scheduled to launch in 2009.[3] However, the technology has several disadvantages for deep-space missions: requirements for powerful lasers, high cost and complexity of the ground operations, and limited coverage. These disadvantages of the ground laser beacon have motivated us to search for other alternative technologies that do not require a laser beacon. Technology options are visible Earth images, thermal Earth images ($\approx$8–13 μm), and stars. One major drawback of the visible Earth images technology is its sensitivity to albedo variation [3] and phase dependence [4]. The thermal Earth image is expected to overcome the albedo and phase dependence of the visible Earth image [5]. The star tracker-based ATP has several distinctive advantages over other methods: range independence, inheritance of mature star tracker technology, and high link availability (no Sun–Earth–probe (SEP) angle dependence). The concept and some preliminary studies were first presented in [4]. On the other hand, the low signal photon count, the main drawback limiting the bandwidth of tracking/pointing servo control if only a star tracker is used, requires the use of accurate and high-bandwidth inertial sensors (gyros or angle sensors). The combination of the star tracker and the inertial sensors can give both the high accuracy and the high-bandwidth pointing knowledge needed for precision deep-space optical communications. The required high pointing-knowledge accuracy is achieved through the iterative averaging process, where the most recent pointing-knowledge (attitude) estimate is averaged with the new star tracker information and bias terms for the inertial sensor are estimated.

The outline of this article is as follows: Section II presents the concept of the star tracker-based ATP technology. Section III discusses the pointing-knowledge estimation method, with the example accuracies given in Section IV. In Section V, we present several options for the star tracker configurations. The link availability is discussed in Section VI. In Section VII, the optical throughput requirement for the 5-Hz star tracker is discussed.

II. ATP Concept Using Star Trackers and Inertial Sensors

Our general approach is to determine both the attitude of the optical communications terminal (OCT) coordinate frame and the receiving station location in inertial space, such as relative to the J2000 coordinate frame (or the newer International Celestial Reference System (ICRS) frame), and to point to a derived location in the optical communications frame. This approach is akin to that used to point science cameras on a Voyager-, Galileo-, or Cassini-type spacecraft. *A specific approach to attaining this attitude (or pointing) knowledge accuracy is to use a combination of high-precision star tracker measurements combined with high-bandwidth inertial sensor updates.* Two types of inertial sensors are assumed: gyros for medium bandwidth (<50 Hz) and angle sensors for high bandwidth (>50 Hz). Additional data, such as spacecraft position from the navigation system, alignment data from in-flight calibrations, and data provided from communication with the ground, are all required to determine the pointing direction (Fig. 1).

The ATP functions perform the measurements and pointing control of the downlink laser signal from the spacecraft platform to the Earth-based receiving station. The key steps of this task are

[3] A. Biswas, S. Lee, G. G. Ortiz, M. Srinivasan, S. Piazzolla, A. Abramovici, D. Losh, C. Lee, and A. Gray, *Pointing, Acquisition and Tracking (PAT) Concept Review for Palomar Receive Terminal (PRT)* (internal document), Jet Propulsion Laboratory, Pasadena, California, August 2004.

(1) Acquisition. Process spacecraft attitude measurement data to determine the initial pointing direction of the system. This information will be used for the initial acquisition of the celestial reference (CR) targets and for determining the twist about the optical boresight. One problem with this is maintaining the alignment knowledge between the spacecraft and optical communications terminal.

(2) Acquire the stars using a focal-plane array—typically a charge-coupled device (CCD).

(3) Tracking measurement update. Determine the optical boresight coordinate frame in the ICRS (or J2000) coordinates based on knowledge of the absolute location of celestial references (based on ephemeris) and measurements captured with a celestial reference detector. This process combines image measurements performed at low-bandwidth discrete sampling times and the corresponding J2000 position to determine the pointing of the OCT with respect to inertial space (i.e., the coordinate transformation). At the discrete sampling times, the attitude estimates are computed and used to update the telescope pointing knowledge.

(4) Attitude propagation. Inertial sensors, typically high bandwidth, are used to fill in attitude updates between the measurement updates of star trackers.

(5) Pointing-direction determination. Determine the desired pointing direction in inertial coordinates, based on ephemeris, one-way light-time, and Earth receiving-station location.

(6) Pointing control. Control a fine-steering mirror to point the downlink laser to the Earth receiving-station direction. This pointing control loop needs to compensate for the effects of line-of-sight and mirror jitter, which is caused by either the vibration of the platform coupling across the mechanical interface or by the mechanical resonance of the structure.

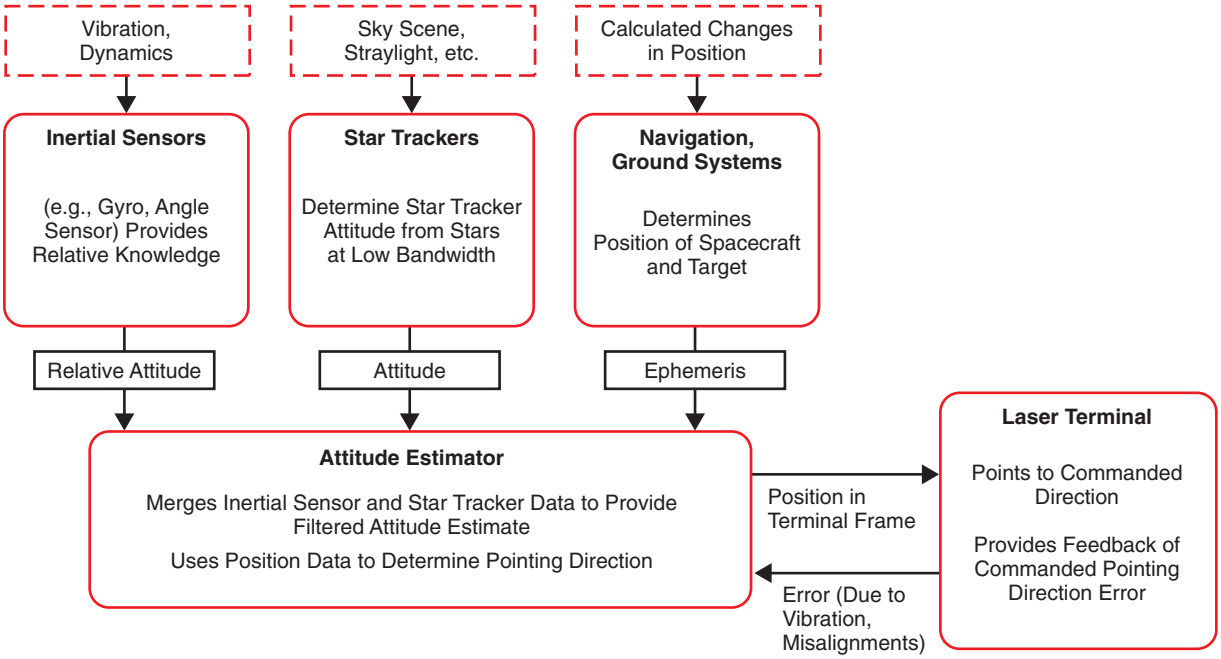

Fig. 1. Functional block diagram of the star-tracker-based ATP system.

III. Pointing-Knowledge Estimation Method

As a blanket statement, the pointing knowledge should be accurate, and the estimated update rate needs to be sufficiently high to compensate the platform vibration. Our goal is to meet these two requirements, high accuracy and update rate, using the combination of star trackers and inertial sensors. Star trackers are very accurate and provide accurate pointing knowledge with typically a low update rate (depending on the star magnitude). On the other hand, inertial sensors can provide relative pointing knowledge with a high update rate. Here we describe how to combine the star tracker and inertial sensors, specifically gyro measurements to reduce the jitter. This method is based on an averaging technique. Angle sensor measurements are used to fill in between the two successive gyro measurements for a higher update rate, and the total root-mean square (rms) error (or jitter) increases in a root-sum-squared (rss) sense.

A. Assumptions for the Jitter Estimation Procedure

Assumptions for the jitter estimation procedure (after the initial acquisition of stars) are as follows:

(1) A one-dimensional discrete time example is assumed. (The estimation works the same way in two or three dimensions, except that it is mathematically more complex.)

(2) The gyro is assumed to be high bandwidth, to have random noise, and to be bias consistent with high-precision gyros. The "high bandwidth" is assumed to be high enough compared to the platform disturbances.

(3) The equations shown depend primarily on the information rate, which is a measure of the signal-to-noise ratio per unit time. Information rate is a method with which, to first order, we can compare the net effect of star trackers with different accuracies and update rates, such as noting that 100 measurements/second with $\sigma^2 = 100$ are the same as 1 measurement with an accuracy of $\sigma^2 = 1 (= 100/100)$.

(4) The star tracker is at a lower frequency. In this example, a tracker measurement is made at every N steps of the gyro. The tracker has random noise, s_k, with variance (assumed to be constant in this case), σ_S^2, and the star tracker measurement propagated to the correct time for inclusion in the estimate (and the σ_S^2 includes any additional noise due to propagation, such as gyro bias contributions).

(5) In this example, the initial estimate of the attitude, x_0, with variance, σ_{x0}^2, is assumed to be based on the star tracker measurement.

(6) The gyro angle measurement is g_k. We assume there is an estimation state (not shown) for bias, and the measurement is compensated for the estimated bias:

   (a) The random error (angle random walk, assumed to contain a priori uncertainty due to gyro bias) is w_k, with variance σ_w^2 (degrees^2/hour).

   (b) Bias error is b_k (degrees/hour), with a mean value b over the short interval in question.

   (c) The only bias-error contribution is due to the residual bias error.

(7) Assume uniform time spacing Δt seconds between successive gyro measurement updates and uncorrelated error sources, with N measurements of the gyro between every star tracker update. The star tracker measurements are then $T = N\Delta t$ seconds apart.

(8) After k steps, x_k will be the pointing estimate for the gyro.

B. Basic Equations

To estimate the attitude of the one-dimensional telescope boresight, x_k,

$$E[w_k] = 0 \qquad \text{white noise}$$

$$\theta_0 = x_0 \qquad \text{initial state}$$

$$\theta_{k+1} = \theta_k + (g_k + w_k) \quad \text{gyro based state equation}$$

and the change in error, which includes residual bias error, is

$$e_{k+1} = e_k + w_k + \Delta t^* b_k \tag{1}$$

and the total error becomes (with bias and noise)

$$E\left[(e_{k+1})^2\right] = \Delta t \sigma_w^2 + (\Delta t\, b_k)^2 + E\left[(e_k)^2\right] \text{ (degrees}^2\text{)} \tag{2}$$

Then for N steps, the total error becomes

$$E\left[(e_{k+N})^2\right] = N\Delta t\, \sigma_w^2 + (N\Delta t\, b_k)^2 + E\left[(e_k)^2\right] \tag{3}$$

The variance (after taking out the mean error, $(N\Delta t\, b_k)^2$, is

$$\text{Var } (e_{k+N}) = \text{Var } (e_k) + N\Delta t\, \sigma_w^2 \tag{4}$$

The increase in the total error is approximately $N\Delta t\, \sigma_w^2$ (jitter) + $(N\Delta t\, b)^2$ (bias) between measurements N and $N + k$.

Without any star tracker measurements, the estimated attitude angle is

$$x_k = \theta_k, \quad \text{Var}(x_k) = \text{Var}(e_k) \tag{5}$$

After a star tracker measurement, using standard-type Kalman filter/least-squares weighting to incorporate the star tracker measurement, and with a defined by

$$a = \frac{\sigma_S^2}{\sigma_S^2 + \text{Variance}(e_k)} \tag{6}$$

the update (note the superscript $^+$) is made by computing

$$x_k^+ = (s_k)(1 - a) + a x_k \tag{7}$$

$$\text{Var}(x_k^+) = (1 - a)^2 \sigma_S^2 + a^2 \text{ Var}(e_k) = \frac{\text{Var}(e_k) * \sigma_S^2}{\sigma_S^2 + \text{Var } (e_k)} \tag{8}$$

C. Iterative Averaging Process

For $k = 0$ and time $t = 0$, the total error variance is σ_S^2 with $T = N\Delta T$. For $k = N$, before the next tracker update,

$$\text{Var } (x_N) = \text{Var } (x_0) + T\sigma_w^2 = \sigma_S^2 + T\sigma_w^2 \tag{9}$$

and the corresponding bias error is $T\,b$.

After the update with a star tracker measurement, substituting Var (x_N) in Eq. (9) for Var (e_k) in Eq. (8) gives the new variance

$$\text{Var } (x_N^+) = \sigma_S^2 * \frac{T\sigma_w^2 + \sigma_S^2}{2\sigma_S^2 + T\sigma_w^2} \tag{10}$$

For accumulated bias error, substituting Var (x_N) in Eq. (9) for Var(e_k) in the denominator of Eq. (8) and $T\,b$ for Var (e_k) in the numerator of Eq. (8) gives the new estimate

$$\frac{\sigma_S^2}{2\sigma_S^2 + T\sigma_w^2}(T\,b) \tag{11}$$

The derivation process for Eq. (10) is shown in Fig. 2.

At time $t + T$, the new estimate is the average of the star tracker measurement at time t (which has 1-sigma error of σ_S^2) propagated using gyro angle measurements (the propagated star tracker measurement taken at time t has a 1-σ variance of $\sigma_S^2 + T\sigma_w^2$ at time $t + T$) and the new star tracker measurement at time $t + T$ (1-σ variance of σ_S^2). The equally weighted average of the attitude estimate with gyro propagated, x_N, and the star tracker update, x_S, is

$$x_N^+ = \frac{x_N + x_S}{2}$$

Under those assumptions, the variance is

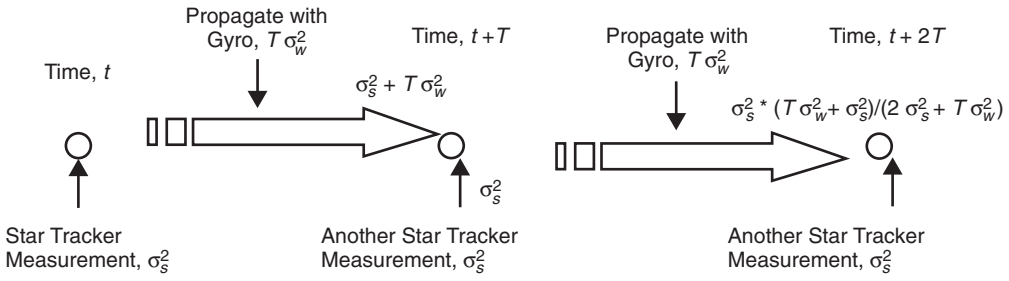

Fig. 2. Iterative averaging process for the pointing knowledge estimation variance.

$$\text{Var } (x_N^+) = \frac{\text{Var } (x_N) + \text{Var } (x_S)}{4}$$

$$= \frac{\sigma_S^2 + T\sigma_w^2 + \sigma_S^2}{4}$$

$$= \frac{2\sigma_S^2 + T\sigma_w^2}{4}$$

However, a more reasonable assumption is to give more weight to the estimate with smaller variance. One method to perform the weighted averaging with the variances is as follows:

$$x_N^+ = \text{Var } (x_N)\frac{x_S}{\text{Var } (x_N) + \text{Var } (x_S)} + \text{Var } (x_S)\frac{x_N}{\text{Var } (x_N) + \text{Var } (x_S)}$$

$$= (T\sigma_w^2 + \sigma_S^2)\frac{x_S}{T\sigma_w^2 + 2\sigma_S^2} + (\sigma_S^2)\frac{x_N}{T\sigma_w^2 + 2\sigma_S^2}$$

then

$$\text{Var } (x_N^+) = (T\sigma_w^2 + \sigma_S^2)^2 \left(\frac{\sigma_S^2}{T\sigma_w^2 + 2\sigma_S^2}\right)^2 + (\sigma_S^2)^2\frac{(T\sigma_w^2 + \sigma_S^2)}{(T\sigma_w^2 + 2\sigma_S^2)^2}$$

$$= \sigma_S^2 * \frac{T\sigma_w^2 + \sigma_S^2}{2\sigma_S^2 + T\sigma_w^2} \tag{12}$$

For a more general case where the attitude estimate at time t is star tracker measurement propagated with gyro measurement, let the attitude estimate be x_u (with the corresponding 1-sigma variance σ_U^2); then the variance of x_N^+ is

$$\text{Var } (x_N^+) = (T\sigma_w^2 + \sigma_U^2)^2\frac{\sigma_S^2}{(T\sigma_w^2 + \sigma_U^2 + \sigma_S^2)^2} + (\sigma_S^2)^2\frac{T\sigma_w^2 + \sigma_U^2}{(T\sigma_w^2 + \sigma_U^2 + \sigma_S^2)^2} \tag{13}$$

After additional N gyro measurements, the error variance grows to

$$\text{Var } (x_{2N}) = \text{Var}(x_N^+) + T\sigma_w^2 \tag{14}$$

IV. Pointing-Knowledge Accuracy

In this section, the ranges of sensor performances are given in terms of jitter and bias error. For the inertial sensors, we surveyed commercial products for the jitter and bias error. For the star tracker, a simulation was used to obtain the jitter estimates. For the bias error of the star trackers, estimates from a narrow field of view (FOV) star tracker design[4] and from one of the best commercially produced star trackers are given.

[4] Ibid.

A. Inertial Sensor Accuracy

1. Gyro Accuracy.

The jitter sources include angle white noise (AWN), angle random walk (ARW), and rate random walk (RRW). Among these jitter sources, ARW is the major error source. Good gyros, such as the Hemispherical Resonator Gyro (HRG), have an ARW of less than 0.0001 deg/rt-hr [7].

For good gyros, the bias instability (drift fluctuations over the operating range of the gyros) has values that are 0.005 to 0.0001 degrees/hour (1 σ) [3]. For setting a requirement, we allocate a 0.1-microradian position error due to bias uncertainty at the end of 15 seconds. It is required that the gyros have an error of less than 0.0015 degrees per hour, which is the total bias drift stability for good gyros; a bias estimator (not shown) will keep the resulting bias error to less than 0.1 microradian, 3 sigma, per axis. Because the bias drift rate changes slowly, there is sufficient time and a sufficient number of tracker measurements to estimate the gyro bias to this degree of accuracy.

2. Angle Sensor Accuracy. For the angle sensor, we assume use of the specific angle sensor made by BEI (Model ADS 8301). The jitter and bias errors are from the specification sheet of this product [6].

Jitter: 30 nrad is the maximum (rms) noise measured from the power spectral density (PSD) over the bandwidth from 2 to 500 Hz with the low operating range of ± 10 μrad.

The major bias error is from the frequency response. The 1-sigma bias for the low range of the BEI angle sensor is ± 2.5 percent. This implies the bias error depends on the spacecraft vibration. For example, the bias error for the Olympus spacecraft (an rms vibration of $\sim$16 μrad) would be 0.4 μrad for a bandwidth up to 300 Hz. Since the angle sensor provides spacecraft vibration from the gyro bandwidth (50 Hz for the examples above), the corresponding rms error would be 40 nrad.

B. Star Tracker Accuracy

Figure 3 gives a bound for the noise equivalent angle (NEA) of a star tracker using a CCD detector with 10e read noise and different centroiding window sizes. The centroiding formula used in this first case was just the "center of mass" algorithm, which results in an NEA that is only a little worse than that from a noise-optimized algorithm. As can be seen, at a 10e read noise per pixel, 3500 electrons will produce a 1/25 pixel NEA for the centroid window of 5×5 pixels. The simulation results added Gaussian noise for read noise and photon statistics, but the rest was assumed to be calibrated (such as the "S-curve").

In addition to the CCD characteristics, there are a number of additional factors that affect star tracker performance. The following is a list of the *external* space environmental factors (input to the tracker) that affect star tracker performance:

(1) Number of stars in the FOV to the limiting instrument magnitude of the tracker.

(2) Distribution of stars relative to the pointing direction; e.g., equally weighted star measurements, the attitude at the barycenter of the stars has the best two-axis accuracy. Given that, where is the desired pointing direction relative to the barycenter?

(3) Interloper stars, planets, optically nearby stars, and non-stellar objects. The tracker algorithms need to account for these disturbance sources.

(4) Positional accuracy of the stars in the reference catalog. For stars brighter than $\sim$9.5 magnitude, we currently can expect to get about 10- to 40-mas (milliarcsecond) accuracy per star ($\sim$50 to 200 nanoradians). This will improve as more astrometric missions are deployed.

(5) Spectral distribution knowledge (color) accuracy. This is needed for determining the point spread function (PSF) shape and algorithm parameters.

(6) Stray light contribution from the Sun, Earth, and bright stars in or near the FOV. Optical surface cleanliness will be a significant issue.

(7) Angular rate of the stars relative to the pixels in the FOV (image smear). Note that Earth moves at 0 to 10 μrad per minute at a distance of 1 AU.

The following are dependent on the tracker hardware characteristics:

(8) Realistic light collection capability. A 10-cm-diameter aperture will collect roughly 400,000 photons/second for a 5000- to 7000-kelvin magnitude 9 star between the wavelengths 400 nm and 1000 nm. The detector conversion and optical losses are important considerations in determining accuracy, and it might be expected that 100,000 to 200,000 photons/second would result.

(9) NEA contribution from each star. This is driven by the end-to-end combination of the centroiding algorithms, electronics noise and detector dark current, and collected light (target star and interfering star). With suitable algorithms, this becomes a "pure" noise source.

(10) Residual optical distortion does not filter over short time periods (hundreds of seconds; it never filters without star field motion on the detector). The residual optical will depend on star color and FOV position (especially when there are many refractive elements), and it has the potential to be a major bias (non-filterable for this application).

(11) Centroiding bias contribution. Note that the phrase "centroiding algorithm" refers to any estimation process for the position (center) of the star, which is based on the focal-plane measurements, and is not restricted to just a center of brightness algorithm. The bias-error term should be interpreted as an rms value over the effective period of averaging. For most centroiding algorithms, an optimistic value to use is a 1-sigma value of 0.7 times the amplitude of the peak bias error per axis, assuming a sine type error, so that the averaging takes place over a full period of the spatial error. In previous work, the optimization of the centroiding algorithms (Astro-1, Cassini, and Starlight) was examined. When filtered, this can result in the 1-sigma error bias realized by the rms error. Incorrect processing can lead to requiring that the peak value of the maximum to minimum errors (2$\times$ amplitude) as a star moves over 1/4 of a pixel be used as the error term.

The star tracker bias error sources include time-tag latency/jitter, modeling error (stellar spectral distribution, CCD spectral response, and PSF distribution), modeling limitations, spot angular rate uncertainty (smear compensation), image truncation (centroid area loss), and spot smear due to angular rate acceleration. Some of these errors can be corrected to a certain degree. The uncorrected error becomes the residual bias error.

Table 1 shows surveyed results from three commercial star trackers[5] and design estimates from a high-resolution star tracker.[6]

Star tracker performance generally depends on the number of stars in the FOV, which is related to the star tracker FOV location relative to the galactic plane (Milky Way).

[5] G. G. Ortiz, *Deep Space Conceptual Design*, Space Technology 6 Midterm Presentation (internal document), Jet Propulsion Laboratory, Pasadena, California, May 2001.

[6] J. W. Alexander, "Starlight Camera Error Budget and Analysis," JPL Interoffice Memorandum (internal document), Jet Propulsion Laboratory, Pasadena, California, April 2002.

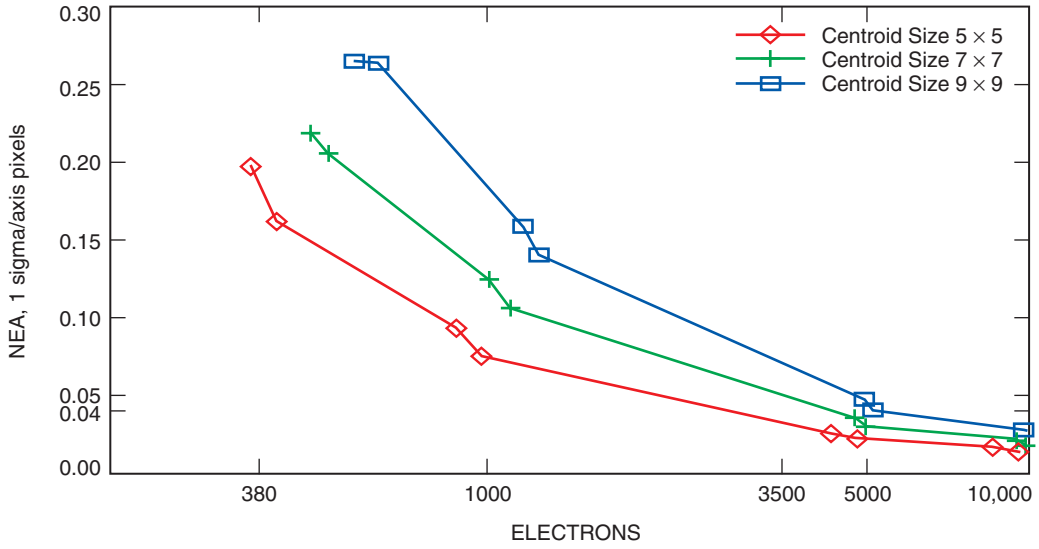

Fig. 3. NEA versus signal and centroid window for a 10e read noise.

Table 1. Surveyed star tracker performances.

Star tracker	Specification bias, nrad (1 σ/axis)	Best estimate bias, nrad (1 σ/axis)	Specification NEA, nrad (1 σ/axis)	Best estimate NEA, nrad (1 σ/axis)	Comments
SIRTF	3010	1460	1070	490	25 to 40 stars, 5×5 deg FOV
Aspect camera assembly	1000	530	1750	310	Ball Aerospace, 1.4×1.4 deg FOV, 1 to 5 stars
SSP	500	300	750	300	Ball Aerospace, 8.8×8.8 deg FOV
Starlight camera	—	50	—	600	11 μrad/pixel, narrow FOV camera

C. Pointing-Knowledge Accuracy

Figure 4 shows the noise reduction cases due to averaging from the use of gyros with the star tracker measurements. There are six shown: using gyros with random walk (ARW) values of 0.0001 and 0.001 degrees/hr$^{1/2}$, ignoring the bias growth, and assuming a 5-hertz tracker with noise values of 2, 1, and 0.7 microradians per frame (1 sigma).

Figure 4 shows that with propagation of 5 seconds or more, an accuracy better than 0.5-microradian can be achieved. With SIRTF-class gyros (ARW = 0.0001 deg/root-hr), and a 0.7-microradian/frame tracker, 150-nanoradian accuracy is achieved in 5 seconds of averaging. As is obvious, the better the tracker, the worse the gyros can be.

If the star tracker update rate is increased, the jitter decreases due to shorter propagation time (Fig. 5). If angle sensor jitter is combined with the star tracker–gyro jitter, then the total 1-sigma pointing-knowledge error would be slightly higher, as shown in Fig. 6.

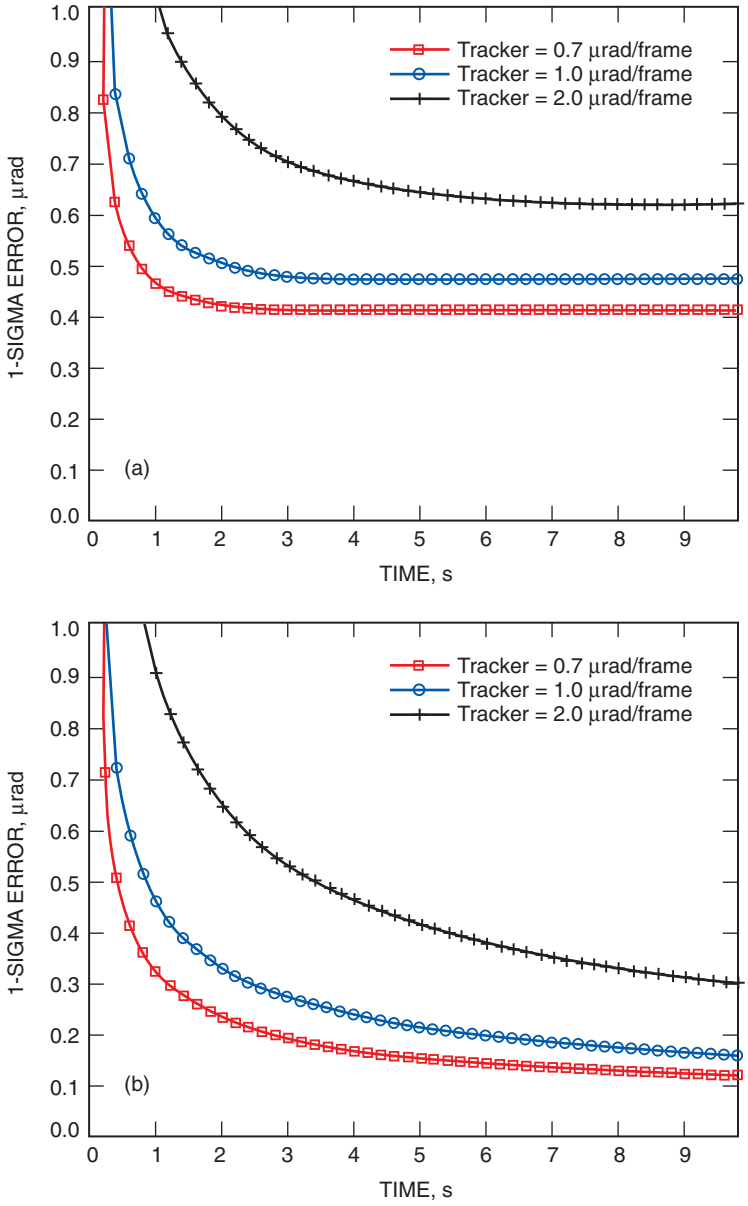

Fig. 4. Iterative averaging process as a function of propagation time for a star tracker rate of 5 Hz: (a) ARW = 0.001 deg/root-hr and (b) ARW = 0.0001 deg/root-hr.

V. Configurations

In this section, we compare two star tracker configurations in terms of accuracy and star coverage.

A. The Single Star Tracker Approach

A single star tracker gives two good attitude estimates (x- and y-axes) and one poor attitude estimate (the twist around the boresight) because of the lack of star separation from the center of the FOV. Typically for narrow-angle star trackers, the attitude estimates on the twist around the boresight are about 20 times worse than those of the other axes. Therefore, the star tracker orientation relative to the

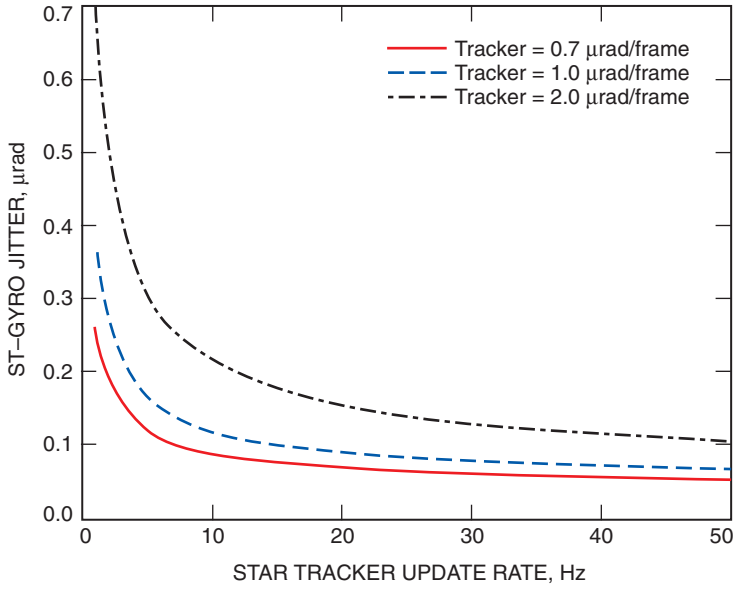

Fig. 5. Star tracker–gyro combined jitter as a function of star tracker measurement update rate for the ARW = 0.0001 deg/root-hr.

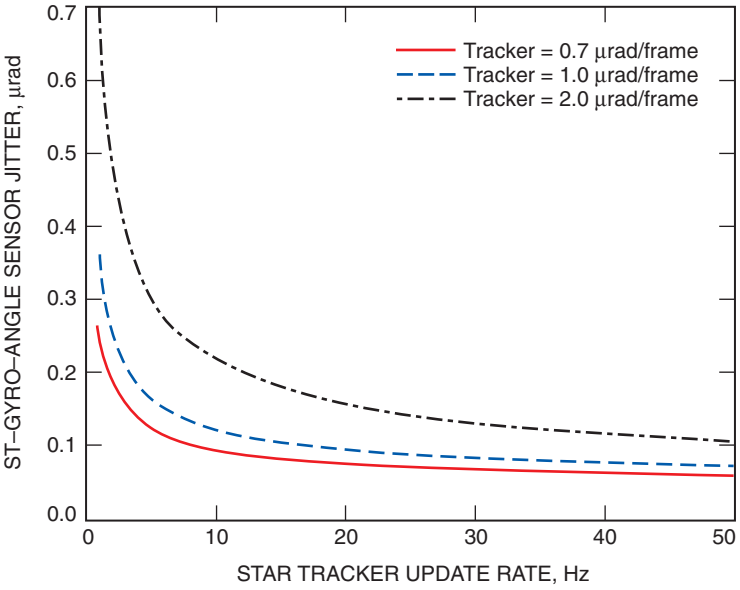

Fig. 6. Star tracker–gyro–angle sensor combined jitter as a function of star tracker measurement update rate for the ARW = 0.0001 deg/root-hr.

optical communication terminal is critical. To take advantage of this fact, the star tracker will be aligned along the communication terminal, either facing the Earth receiver (boresighted) or 180 degrees, facing the opposite direction (antipodal). Due to the Sun's stray light issue, antipodal is the preferred configuration. One potential issue with the single star tracker approach is the relatively low star availability due to the limited star search area. However, this availability heavily depends on the actual mission profile. As will be shown in Section VI, the average sky coverage with a single star tracker is better than 98 percent. Therefore, the maximum difference in available pointing directions is 2 percent or less on average.

B. The Two (or Multi-FOV) Star Tracker Approach

Since the boresight-twist estimation is large, a common approach is to use multiple star trackers. Some implementations use separate, independent trackers; there are other designs that use mechanically integrated trackers and others that use multiple FOVs (such as the mini-owls) on a single detector. Another strength of the two star tracker approach is the enhanced star coverage as compared with the single star tracker. With multiple tracker FOVs, the key issues become

(1) Alignment knowledge between tracker FOVs

(2) Alignment knowledge between trackers and the pointing direction

(3) Star availability in each FOV

The alignment between a pair of continuously operated star trackers is almost automatic. Otherwise, changes in alignment cannot be attributed to changes to either tracker.

Table 2 summarizes the four configuration options with the pros and cons of each configuration.

VI. Link Availability

The link availability of the star tracker-based ATP system directly depends on the star coverage. In this subsection, the star coverage is discussed in detail.

A. Coordinate Frames—Where Are All the Stars?

Defining three coordinate frames may help to explain some of the usual (sometimes misunderstood) star tracker considerations. First, the J2000 frame (or the ICRS frame), which uses the familiar right

Table 2. Pros and cons of the four configuration options for the star-tracker-based ATP system.

Star tracker orientation (relative to optical communications telescope)	Pros	Cons
Antipodal	Looks away from Earth; more stars without Earth in FOV. Generally no Sun problems for outer planets; lower twist error contribution to pointing. Best pointing direction in the telescope direction.	Places more restrictions on mounting, requiring unrestricted viewing area, especially if mounted on the same platform as optical communications terminal. Requires accurate alignment with telescope pointing optics and needs to develop calibration procedure.
Boresighted	Shares channel; lower twist error contribution to pointing. Common optics relaxes alignment requirements.	Earth blocks out stars in partial FOV. Sun increases background and stray light so that long baffle may be required.
Normal	Can be rotated with spacecraft for greatest star coverage field of regard.	Large error in one line-of-sight axis (can be reduced with two star trackers) due to large star tracker twist error.
Gimbaled	Can be pointed and slewed to particular star or celestial body.	Requires gimbal mechanism; twist error about star tracker boresight may cause large pointing errors as boresight moves away from antipodal pointing. Knowledge of gimbaled position introduces additional error source.

ascension (RA) and declination (DEC), with dec = 90 degrees for the North Pole, and the J2000 equatorial plane (defined by the North Pole) being parallel to the plane of the Earth's Equator.[7] Second, the ecliptic coordinate frame, with the ecliptic plane containing the orbit of the Earth about the Sun (which is also close to the orbits of the other planets). Finally, the galactic coordinate frame, where the galactic plane contains the bulk of the Milky Way (which has a very high density of stars). The North Pole unit vectors for the galactic and ecliptic coordinate frames (+z-axis) are expressed in J2000 coordinates as

$$\text{north galactic pole} = (-0.867665 \quad -0.198076 \quad 0.455985)$$

$$\text{north ecliptic pole} = (\quad 0 \quad -0.397777 \quad 0.917482)$$

$$\text{north J2000 pole} = (\quad 0 \quad 0 \quad 1)$$

The angle between the J2000 equatorial plane and the galactic equatorial plane is about 60.2 degrees, and between the ecliptic and the J2000 equator it is about 23.4 degrees.

Most spacecraft stay close to the ecliptic plane (all the planetary missions, for example). The star density is largest in the galactic plane and least at the poles by roughly a factor of 4.

B. Star Coverage Analysis

Star coverage (star availability) is presented in this section. Data analysis was based on star position and visual magnitude data that were extracted from the Tycho II star catalog. A computer program was constructed that centered a circular FOV of 3.5-, 4.0-, 4.5-, 5.0-, 5.5-, and 6-degree diameter at each point of an RA (α) and declination (δ) grid defined on the celestial sphere. The spacing of the grid was 0.1 degree in both RA and declination. For each combination of position (α, δ), FOV size, and cutoff magnitude, the number of stars found within the FOV was computed. Finally, as a function of FOV size, the fraction of the sky where the specified number of stars is obtained is computed as a function of magnitude. Tables 3 through 5 provide a snapshot for the star magnitude cutoff needed to achieve 98 percent sky coverage, and of predicted performance as a function of FOV and the number of stars with the specified visual magnitude. In the tables, red (or bold-faced) values show the conditions where 99 percent of the sky has coverage. In computing the predicted performance, we assume that each star above the specified magnitude that lies within the circular FOV will give exactly 1/25 pixel NEA, and that the FOV is exactly 1000 by 1000 pixels, without considering the aperture size or number of photons required to achieve 1/25 pixel accuracy. This is reasonable, and it possibly is conservative with a very low noise detector and if brighter stars are given more weight.

VII. Optical Throughput Requirements

In this section, the star tracker optical throughput requirements are discussed. The requirements are to provide 4000e/frame for 1/25th pixel centroiding NEA. There are a number of possible tracker configurations as well as detector/quantum efficiency (QE) and signal-to-noise requirements. The larger the aperture, the more photons per second. The better the QE or lower the detector noise, the smaller the number of photons required. The magnitude cutoff was computed, based on 50 percent photons-to-electrons throughput, for the cases of 2000e/frame/star and 4000e/frame/star.

Table 6 identifies three cases: case 1, for a 5.7-cm diameter, optimistically gives 4000 photons, assuming 2000e per frame, and tracks stars to 9.25-V magnitude; case 2, for an 8-cm diameter, conservatively gives

[7] In reality, the ICRS coordinate frames are defined by distant stars and were initialized to match the Earth J2000-based parameters.

Table 3. Star count and magnitude cutoff versus FOV size needed to achieve 98% of the sky coverage.

count	5	10	16	25	36	49	64	81	100	121	144	169	200
FOV (deg)													
3.5	8.5	9.0	9.5	9.5	10.0	10.5	11.0	11.0	11.5	11.5	11.5	***	***
4.0	8.0	8.5	9.0	9.5	10.0	10.0	10.5	10.5	11.0	11.0	11.5	11.5	***
4.5	8.0	8.5	9.0	9.5	9.5	10.0	10.0	10.5	10.5	11.0	11.0	11.5	11.5
5.0	8.0	8.5	8.5	9.0	9.5	9.5	10.0	10.0	10.5	10.5	11.0	11.0	11.5
5.5	7.5	8.0	8.5	9.0	9.5	9.5	10.0	10.0	10.5	10.5	10.5	11.0	11.0
6.0	7.5	8.0	8.5	9.0	9.0	9.5	9.5	10.0	10.0	10.5	10.5	10.5	11.0

Table 4. Performance estimate, assuming 1000 pixels across the detector and 1/25 pixel random error/star/axis attached to each measurement. The performance is reported in microradians 1σ, per axis, worst-case rms for 98% of the sky. There is a 1:1 correspondence between this and Table 3.

count	5	10	16	25	36	49	64	81	100	121	144	169	200
FOV (deg)	Accuracy 1σ/axis μrad												
3.5	1.09	0.77	0.61	0.49	0.41	0.35	0.31	0.27	0.24	0.22	0.20	0.19	0.17
4.0	1.25	0.88	0.70	0.56	0.47	0.40	0.35	0.31	0.28	0.25	0.23	0.21	0.20
4.5	1.40	0.99	0.79	0.63	0.52	0.45	0.39	0.35	0.31	0.29	0.26	0.24	0.22
5.0	1.56	1.10	0.87	0.70	0.58	0.50	0.44	0.39	0.35	0.32	0.29	0.27	0.25
5.5	1.72	1.21	0.96	0.77	0.64	0.55	0.48	0.43	0.38	0.35	0.32	0.30	0.27
6.0	1.87	1.32	1.05	0.84	0.70	0.60	0.52	0.47	0.42	0.38	0.35	0.32	0.30

8000 photons, assuming 4000e per frame, and tracks stars to 9.25-V magnitude; and the case 3 optimistic configuration tracks stars to magnitude 10 for an 8-cm aperture, 2000e per image/frame.

VIII. Conclusion

With the combination of commercially available star trackers and inertial sensors, we have shown that accurate and high-bandwidth pointing knowledge on the order of 150 nrad can be achieved (single axis, 1 sigma) with reasonable assumptions on the system parameters, including the telescope aperture size, star tracker accuracy, gyro accuracy, angle sensor accuracy, star tracker update rate, FOV, and star magnitudes. The estimated pointing knowledge is well below the typical deep-space optical communications requirements of ∼200 to 300 nanoradians. The key concept is to use star trackers for low-bandwidth, gyros for medium-bandwidth, and angle sensors for high-bandwidth pointing-knowledge estimation. An iterative averaging process was derived as one method to combine the star tracker and gyro measurements. One critical parameter, link availability, can be 98 percent or better using the single star tracker. With a two-star tracker approach, link availability can be improved to 100 percent.

Table 5. FOVs of 3.5, 4.0, and 5.5 degrees. Note that the final line for each FOV gives the star magnitude cutoff where 99% of the sky satisfies that condition.

3.5 deg FOV

Magcut	5	10	16	25	36	49	64	81	100	121	144	169	200
5.0	.000	0	0	0	0	0	0	0	0	0	0	0	0
5.5	.004	0	0	0	0	0	0	0					
6.0	.019	.000	0	0	0	0	0	0					
6.5	.096	.005	.001	0	0	0	0	0					
7.0	.345	.034	.004	.000	0	0	0	0	0	0	0	0	0
7.5	.710	.205	.032	.004	.001	0	0	0	0	0	0	0	0
8.0	.948	.600	.218	.040	.007	.002	.000	0	0	0	0	0	0
8.5	.996	.935	.652	.265	.082	.019	.005	.001	.001	.000	0	0	0
9.0	.999	.994	.958	.714	.361	.170	.068	.020	.006	.003	.001	.001	.000
9.5	1(-)	.997	.996	.980	.839	.528	.302	.178	.096	.040	.015	.006	.003
10.0	1	.999	.996	.996	.992	.928	.749	.492	.330	.222	.149	.093	.046
10.5	1	1	.998	.996	.996	.995	.980	.902	.750	.564	.411	.301	.222
11.0	1	1	1	.999	.996	.996	.996	.995	.977	.910	.803	.676	.518
11.5	1	1	1	1	1	.997	.996	.996	.996	.995	.987	.938	.852
12.0	1	1	1	1	1	.997	.996	.996	.996	.995	.987	.938	.852
	8.5	9.0	9.5	10.0	10.0	10.5	11.0	11.0	11.5	11.5	20.0	20.0	20.0

0.17 of the sky has 49 stars if we allow a cutoff of magnitude 9.0

4.0 deg FOV

Magcut	5	10	16	25	36	49	64	81	100	121	144	169	200
5.0	.001	0	0	0	0	0	0	0	0	0	0	0	0
5.5	.008	.000	0	0	0	0	0	0	0	0	0	0	0
6.0	.043	.001	0	0	0	0	0	0	0	0	0	0	0
6.5	.184	.012	.001	.000	0	0	0	0	0	0	0	0	0
7.0	.521	.087	.009	.001	0	0	0	0	0	0	0	0	0
7.5	.868	.367	.091	.012	.002	.000	0	0	0	0	0	0	0
8.0	.983	.813	.401	.112	.023	.005	.001	.000	0	0	0	0	0
8.5	.998	.983	.865	.470	.194	.065	.018	.005	.002	.001	.000	0	0
9.0	1(-)	.997	.992	.910	.616	.315	.168	.076	.026	.009	.004	.002	.001
9.5	1	.999	.997	.995	.966	.810	.524	.313	.202	.122	.063	.026	.010
10.0	1	1(-)	.998	.996	.995	.987	.928	.779	.552	.373	.264	.190	.127
10.5	1	1	1	.998	.996	.996	.993	.984	.926	.812	.664	.496	.356
11.0	1	1	1	1	1(-)	.997	.996	.996	.995	.987	.948	.871	.757
11.5	1	1	1	1	1	1	.999	.997	.996	.996	.996	.994	.970
12.0	1	1	1	1	1	1	.999	.997	.996	.996	.996	.994	.970
	8.5	9.0	9.0	9.5	10.0	10.5	10.5	11.0	11.0	11.5	11.5	11.5	20.0

4.5 deg FOV

Magcut	5	10	16	25	36	49	64	81	100	121	144	169	200
5.0	.002	0	0	0	0	0	0	0	0	0	0	0	0
5.5	.014	.000	0	0	0	0	0	0	0	0	0	0	0
6.0	.074	.003	.000	0	0	0	0	0	0	0	0	0	0
6.5	.287	.023	.003	.000	0	0	0	0	0	0	0	0	0
7.0	.674	.165	.022	.002	.000	0	0	0	0	0	0	0	0
7.5	.939	.541	.177	.027	.005	.001	0	0	0	0	0	0	0
8.0	.990	.916	.600	.217	.056	.013	.003	.001	.000	0	0	0	0
8.5	.998	.992	.953	.681	.331	.143	.047	.014	.004	.002	.001	.000	0
9.0	1(-)	.996	.995	.972	.824	.508	.278	.156	.073	.027	.010	.004	.002
9.5	1	.999	.996	.996	.990	.938	.760	.499	.316	.211	.134	.078	.032
10.0	1	1	.999	.996	.996	.995	.984	.919	.780	.573	.409	.293	.208
10.5	1	1	1	.998	.996	.996	.996	.994	.986	.935	.840	.710	.543
11.0	1	1	1	1	1(-)	.996	.996	.996	.996	.996	.990	.964	.895
11.5	1	1	1	1	1	1	.999	.997	.996	.996	.996	.996	.995
12.0	1	1	1	1	1	1	.999	.997	.996	.996	.996	.996	.995
	8.0	8.5	9.0	9.5	9.5	10.0	10.5	10.5	11.0	11.0	11.0	11.5	11.5

Table 6. Star tracker diameter size versus photon flux for a 5-Hz update rate.

Nearest Spectral Type	Blackbody Temperature (Kelvin)	BC correction	Photons /sec through aperture at Vmag = 9	Wavelength centroid	V mag required for 20000. photons /sec	Diam (cm) for 20000. photons /sec at mag 9
5Hz Tracker Diameter = 5.7 cm20000. photons /sec, Track to Vmag < 9.25						
M6	3000	-2.50	14133	7628	11.12	6.78
K8	4000	-1.00	23842	7236	10.19	5.22
K1	5000	-0.20	28409	6953	9.58	4.78
G0/F8	6000	-0.05	28944	6751	9.45	4.74
F1	7000	-0.05	27266	6604	9.39	4.88
A8	8000	-0.10	24650	6494	9.33	5.13
A4/A3	9000	-0.20	21808	6411	9.29	5.46
A1	10000	-0.30	19084	6346	9.25	5.84
5Hz Tracker Diameter = 8 cm 40000. photons /sec, Track to Vmag < 9.25						
M6	3000	-2.50	27841	7628	11.11	9.59
K8	4000	-1.00	46964	7236	10.17	7.38
K1	5000	-0.20	55962	6953	9.56	6.76
G0/F8	6000	-0.05	57016	6751	9.43	6.70
F1	7000	-0.05	53710	6604	9.37	6.90
A8	8000	-0.10	48557	6494	9.31	7.26
A4/A3	9000	-0.20	42957	6411	9.28	7.72
A1	10000	-0.30	37592	6346	9.23	8.25
5Hz Tracker Diameter = 8 cm 20000. photons /sec, Track to Vmag < 10.0						
M6	3000	-2.50	27841	7628	11.86	6.78
K8	4000	-1.00	46964	7236	10.93	5.22
K1	5000	-0.20	55962	6953	10.32	4.78
G0/F8	6000	-0.05	57016	6751	10.19	4.74
F1	7000	-0.05	53710	6604	10.12	4.88
A8	8000	-0.10	48557	6494	10.06	5.13
A4/A3	9000	-0.20	42957	6411	10.03	5.46
A1	10000	-0.30	37592	6346	9.99	5.84

References

[1] C.-C. Chen and J. R. Lesh, "Overview of the Optical Communications Demonstrator," *Free-Space Laser Communication Technologies VI*, Proceedings of the SPIE, vol. 2123, pp. 85–94, 1994.

[2] T. Tolker-Nielsen and G. Oppenhauser, "In-Orbit Test Result of an Operational Optical Intersatellite Link Between ARTEMIS and SPOT4, SILEX," *Free-Space Laser Communication Technologies XIVI*, Proceedings of the SPIE, vol. 4635, pp. 1–15, 2002.

[3] C.-C. Chen and M. Z. Win, "Effect of Earth Albedo Variation on the Performance of a Spatial Acquisition Subsystem Aboard a Planetary Spacecraft," *Space Sensing, Communications, and Networking*, SPIE, vol. 1059, pp. 52–59, 1989.

[4] J. W. Alexander, S. Lee, and C. Chen, "Pointing and Tracking Concepts for Deep Space Missions," *Free-Space Laser Communication Technologies XI*, Proceedings of the SPIE, vol. 3615, pp. 230–249, 1999.

[5] S. Lee, G. G. Ortiz, W. T. Roberts, and J. W. Alexander, "Feasibility Study on Acquisition, Tracking, and Pointing Using Earth Thermal Images for Deep-Space Ka-Band and Optical Communications," *The Interplanetary Network Progress Report 42-155, July–September 2003*, Jet Propulsion Laboratory, Pasadena, California, pp. 1–18, November 15, 2003.
http://ipnpr.jpl.nasa.gov/tmo/progress_report/42-155/155E.pdf

[6] BEI Technologies, Inc., *Model 8301 Inertial Angular Displacement Sensor Specifications*, Little Rock, Arkansas, 1999.

[7] A. Matthews and D. A. Bauer, "Hemispherical Resonator Gyro Noise Reduction for Precision Spacecraft Pointing," *Advances in the Astronautical Sciences, Guidance and Control*, vol. 92, pp. 83–100, 1996.